for most of the applications. As the directivity depends strongly on the balance of the couplings of two apertures as well as l in Fig. 1(a), the couplings should be made approximately the same to achieve a high directivity. The particular design shown in Fig. 1 is a result of a compromise between the directivity and the bandwidth of the device obtained through a cut-and-try procedure. During the optimization procedure, it was possible to obtain a 36-dB directivity for a much narrower bandwidth of around 33.1 GHz. To achieve a good directivity by using the hole-type coupler over a wide band of frequencies, a coupler with many apertures which have InSb films should be used.

The input VSWR stays below 1.4 over the frequency range from 32 to 36 GHz.

The insertion loss L has the minimum value of 1.0 dB at about 33.2 GHz and 2.5–3 dB at 36 GHz, depending on the applied magnetic field. Although these L values are smaller than the reported values of the insertion loss of other microwave devices using InSb [1], [2], [4], [5], it may be required to reduce the L value and its dependency on the magnetic field for certain applications of the coupler. Our experience shows that L increases with the thickness of the InSb film. The thinnest film that can be prepared by our present technique without sacrificing its electrical properties is about 1 μm.

An inspection of Fig. 3 shows that the coupler has a center frequency of operation at about 33 GHz. This is slightly below the design value of 34.1 GHz at which the separation l of the coupling apertures, referring to Fig. 1, corresponds to three quarters of a guide wavelength. The slight discrepancy may be attributed to the presence of the mica sheets and the finite thickness of the coupling apertures.

The device performance was independent of the input-power level up to 20 mW, which was the limit of the source available at our laboratory.

CONCLUSION

The results obtained for the variable directional coupler at room temperature may be summarized as follows: 1) the coupling varies from 14.2 dB at a 0 magnetic flux density to 40.2 dB at 13 kG, with an average slope of 2 dB/kG; 2) the directivity is larger than about 14 dB over the frequency band of 32–36 GHz; 3) the insertion loss is 1–3 dB for an InSb film thickness of 1 μm; and 4) the variable coupling appears to be achieved by the magnetoresistance effect in the InSb films in the coupling apertures.

Problems left for future studies include: 1) finding relationships between performance characteristics of the coupler and the properties of InSb films; 2) achieving a high directivity over a wide band of frequencies; 3) assessment of the temperature dependence; 4) reduction in the insertion loss; and 5) theoretical analysis to optimize design.

The authors consider that the directional coupler described in this short paper is usable for the shorter millimeter waves, for it employs the evaporated InSb thin films that require a relatively low magnetic field and offer a low insertion loss. The principle also offers a method of trimming the fixed directional coupler with the aid of a permanent magnet, relaxing mechanical tolerance requirements.

ACKNOWLEDGMENT

The authors wish to thank Prof. T. Okabe and Prof. S. Mizushina of Shizuoka University, and Prof. K. Ura of Osaka University for their encouragement in this work.

REFERENCES

[1] K. Suzuki, "Room temperature solid-state plasma nonreciprocal microwave devices," *IEEE Trans. on Electron Devices*, vol. ED-16, pp. 1018–1021, Dec. 1969.
[2] K. Suzuki and R. Hirota, "Nonreciprocal millimeter-wave devices using a solid-state plasma at room temperature," *IEEE Trans. on Electron Devices*, vol. ED-18, pp. 408–411, July 1971.
[3] D. J. White, "Room-temperature Faraday rotation in n-type InSb films at 23.4 GHz," *J. Appl. Phys.*, vol. 39, pp. 5083–5086, Oct. 1968.
[4] T. Okabe, M. Ohshita, and S. Shinohara, "Millimeter-wave isolators with low magnetic field using a thin vacuum-deposited film of InSb," *Trans. IECE of Japan*, vol. 57-B, pp. 244–249, Apr. 1974.
[5] R. J. Dinger, T. M. Waugh, and D. J. White, "Nonreciprocal properties of vacuum-deposited InSb films at 87 GHz," *IEEE Trans. on Microwave Theory Tech.*, vol. MTT-22, pp. 879–880, Oct. 1974.
[6] M. Ohshita, "High electron mobility InSb films prepared by source-temperature-programed evaporation method," *Jap. J. Appl. Phys.*, vol. 10, pp. 1365–1371, Oct. 1971.
[7] R. Levy, *Advances in Microwaves*, vol. 1. New York: Academic Press, 1966.
[8] M. Sucher and J. Fox, *Handbook of Microwave Measurements*, vol. II. New York: Polytechnic Press, 1963.
[9] H. H. Wieder and D. J. White, "Microwave magnetoresistance of dendritic N-type InSb films," *J. Appl. Phys.*, vol. 39, pp. 2401–2407, Apr. 1968.

The Segmentation Method—An Approach to the Analysis of Microwave Planar Circuits

T. OKOSHI, MEMBER, IEEE,
Y. UEHARA, AND T. TAKEUCHI

Abstract—In many practical planar circuitries, the circuit pattern can be divided into several segments which themselves have simpler shapes such as rectangles. The segmentation method proposed in this short paper is a method in which the characteristics of a planar circuit are computed by combining those of the segmented elements. It features a relatively short computer time required. The principle and computer algorithm are described. Finally, as an example, the application of the proposed method to the trial-and-error optimum design of a ladder-type 3-dB hybrid is described.

I. INTRODUCTION

A planar circuit is a 2-dimensional circuit that should be classified between the distributed-constant (1-dimensional) circuit and waveguide (3-dimensional) circuit. It is defined as an electrical circuit having dimensions comparable to the wavelength in two directions, but much less thickness in one direction [1].

Several methods have been known for the analysis of planar circuits. When the circuit pattern is as simple as square, rectangular, circular, or annular, the impedance matrix can be obtained in a series-expansion form from the Green's function of the wave equation [1]. When the circuit pattern is more arbitrary, the numerical analysis based upon the contour-integral representation of the wave equation is most efficient [1]. Other numerical approaches applicable to arbitrary circuit patterns are the variational method, relaxation method, and the finite-element method [2].

When the circuit pattern is entirely arbitrary, we must rely upon one of those numerical analyses. However, in actual planar circuitry, an entirely arbitrary circuit pattern is not very common; in many cases the pattern consists of several "segments," which themselves have simpler shapes such as rectangles.

The "segmentation method" proposed in this short paper is a method in which the characteristics of a planar circuit are
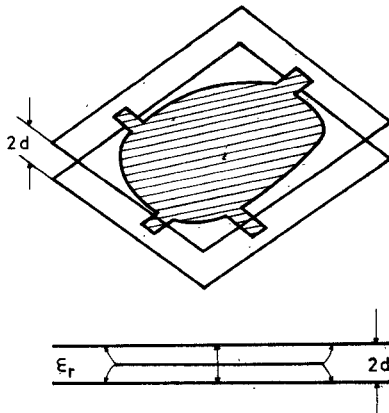
Fig. 1. A triplate-type planar circuit.

computed by combining those of the segmented elements. It features relatively short computer time required in the analysis.

In this short paper, the principle and computer algorithm of the segmentation method are described first in Section II. In Section III, to demonstrate the feasibility of the proposed method, its application to the trial-and-error optimum design of a ladder-type 3-dB hybrid is described as an example. The obtained optimum design is verified by the experiment in Section IV.

II. SEGMENTATION METHOD

A. Basic Concepts

A planar circuit consisting of two ground conductors and a circuit-conductor plate sandwiched by them as shown in Fig. 1 is called a triplate-type planar circuit. In the following only the triplate-type circuit is considered.

The basic equation governing the electromagnetic field in a triplate-type planar circuit is the 2-dimensional wave equation

$$(\nabla_T^2 + k^2)V = 0 \tag{1}$$

where

$$\nabla_T^2 = \frac{\partial^2}{\partial x^2} + \frac{\partial^2}{\partial y^2}, \qquad V = E_z d, \qquad k^2 = \omega^2 \varepsilon \mu$$

ε and μ denote the permittivity and permeability of the spacing material, ω the angular frequency, d the spacing between conductors, and E_z denotes the electric-field strength normal to the conductors.

To analyze such a circuit means to solve the wave equation under given boundary conditions, and determine the circuit parameters of its equivalent n-port network as functions of the frequency. When the circuit pattern is simple (for instance, rectangular), the problem may be solved analytically [1]. The segmentation method is a method of the analysis suited to somewhat more complex patterns, as shown in Fig. 2(a). We divide such a circuit pattern into simpler segments, as shown in Fig. 2(b), compute the characteristics of each rectangular segments from their Green's functions [1], and finally obtain the characteristics of the entire circuit by synthesizing the characteristics of the segments.

B. Interface Network

To facilitate the synthesis of the segments in a unified manner, a new circuit called the "interface network" is introduced. As shown in Fig. 2(c), all connections between segments are made through this interface network. The interface network is nothing but a directly connecting network; it only connects directly those
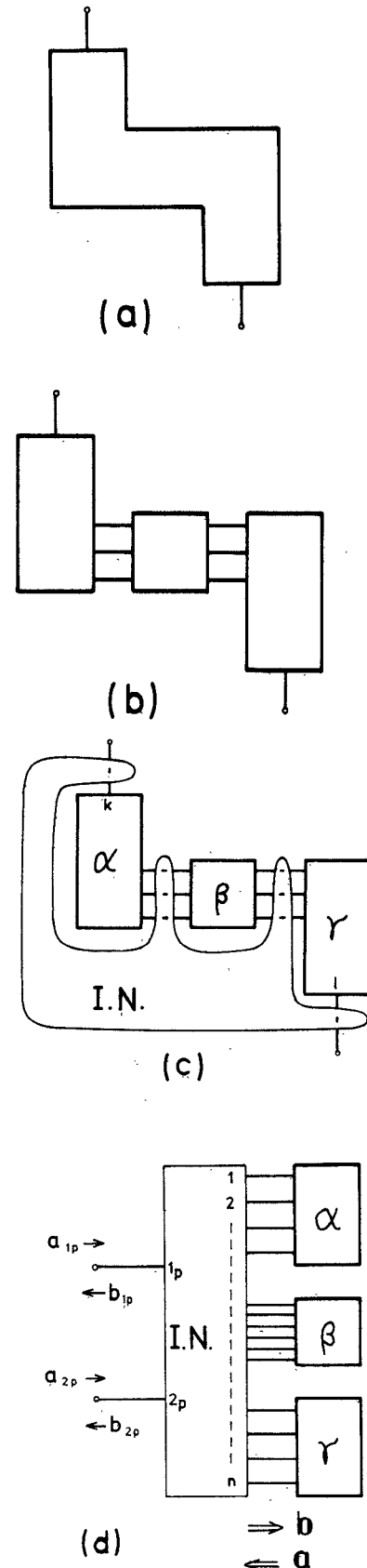

Fig. 2. Principle of the segmentation method. (a) An example of a circuit pattern to which the segmentation method is suitable. (b) Dividing into segments. (c) Introducing the interface network (I.N.). (d) A modified representation of Fig. 2(c).

couples of ports facing each other, as shown in Fig. 2(c). However, a unified formulation of the synthesis is only possible with the aid of this fictitious network.

In the following, we consider a two-port circuit for the simplicity of the formulation. Fig. 2(c) may also be expressed as Fig. 2(d). We define, with respect to ports $1p,2p,1,2,\cdots,n$, incident and reflected waves of the interface network as

$$a_{1p},a_{2p},a_1,a_2,\cdots,a_n$$

and

$$b_{1p},a_{2p},b_1,b_2,\cdots,b_n.$$

In numbering ports, we use (numerals + p) for those of the interface network connected to external ports, and simple numerals for those connected to segmentary circuits.

The aforementioned incident and reflected waves are related in terms of the scattering matrix S_N of the interface network as

$$\begin{bmatrix} b_{1p} \\ b_{2p} \\ b_1 \\ b_2 \\ \vdots \\ b_n \end{bmatrix} = [S_N] \begin{bmatrix} a_{1p} \\ a_{2p} \\ a_1 \\ a_2 \\ \vdots \\ a_n \end{bmatrix} \tag{2}$$

where elements of $[S_N]$ are given by

$$[S_N]_{i,j} = \begin{cases} 1, & \text{if ports } i \text{ and } j \text{ are connected} \\ 0, & \text{if ports } i \text{ and } j \text{ are not connected} \end{cases} \tag{3}$$

where $i,j = 1p,2p,1,2,\cdots,n$. When $i = j$, $[S_N]_{i,j} = 0$.

C. Computation of S-Matrix

If ports $1p$ and $2p$ are connected directly in the interface network to ports k and l, respectively, S_N may be expressed as

$$[S_N] = \begin{bmatrix} 0 & 0 & S_1^{\rightarrow} \\ 0 & 0 & S_2^{\rightarrow} \\ S_1^{\downarrow} & S_2^{\downarrow} & S_n \end{bmatrix} \tag{4}$$

where $S_1^{\rightarrow}$ and $S_2^{\rightarrow}$ are row vectors, and $S_1^{\downarrow}$ and $S_2^{\downarrow}$ are column vectors defined by

$$S_1^{\rightarrow} = (0,\cdots,0,\underset{k}{1},0,\cdots,0)$$

$$S_2^{\rightarrow} = (0,\cdots,0,\underset{l}{1},0,\cdots,0) \tag{4a}$$

$$S_1^{\downarrow} = [S_1^{\rightarrow}]^t$$

$$S_2^{\downarrow} = [S_2^{\rightarrow}]^t \tag{4b}$$

where the superscript t denotes transposition. The submatrix S_n in (4) expresses connections between segments.

The S-matrix of the entire circuit should be a (2×2) matrix giving b_{1p} and b_{2p} in terms of only a_{1p} and a_{2p}. However, we should note that, because $1p$ and $2p$ are connected to k and l, respectively,

$$b_{1p} = a_k \qquad b_{2p} = a_l \tag{5}$$

hold. Therefore, in the following we compute a_k and a_l in terms of a_{1p} and a_{2p}.

From (2), taking out n rows from the bottom, we obtain

$$\begin{bmatrix} b_1 \\ b_2 \\ \vdots \\ b_n \end{bmatrix} = [S_n] \begin{bmatrix} a_1 \\ a_2 \\ \vdots \\ a_n \end{bmatrix} + S_1^{\downarrow} a_{1p} + S_2^{\downarrow} a_{2p}. \tag{6}$$
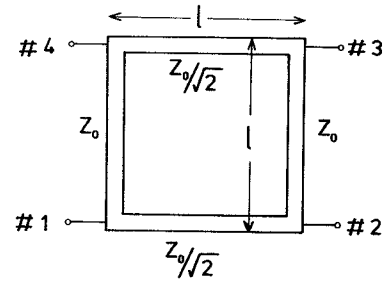

Fig. 3. Basic configuration of a ladder-type 3-dB hybrid circuit.

On the other hand, we may also write

$$\begin{bmatrix} a_1 \\ a_2 \\ \vdots \\ a_n \end{bmatrix} = [S_c] \begin{bmatrix} b_1 \\ b_2 \\ \vdots \\ b_n \end{bmatrix} \tag{7}$$

where S_c is the composite S-matrix of the segmentary circuits expressed as

$$[S_c] = \begin{bmatrix} S_\alpha & & 0 \\ & S_\beta & \\ 0 & & S_\gamma \end{bmatrix} \tag{8}$$

S_α, S_β, and S_γ denoting S-matrices of the segments. When the segments are rectangular these matrices are obtainable analytically [1, eq. (20)].

Eliminating the b-vector from (6) and (7), we obtain

$$\begin{bmatrix} a_1 \\ a_2 \\ \vdots \\ a_n \end{bmatrix} = TS_1^{\downarrow} a_{1p} + TS_2^{\downarrow} a_{2p} \tag{9}$$

where

$$T = [E - S_c S_n]^{-1} [S_c] \tag{9a}$$

E denoting an $(n \times n)$ unit matrix. From (4b)

$$TS_1^{\downarrow} = \text{the } k\text{th column of } T$$

$$TS_2^{\downarrow} = \text{the } l\text{th column of } T. \tag{10}$$

Putting (5) into (9), we finally obtain

$$b_{1p} = a_k = T_{kk}a_{1p} + T_{kl}a_{2p}$$

$$b_{2p} = a_l = T_{lk}a_{1p} + T_{ll}a_{2p}. \tag{11}$$

Equation (11) shows that the S-matrix of the entire circuit is a (2×2) submatrix of T; it consists of four elements of T at crosspoints between the kth, lth columns, and the kth, lth rows. Thus the circuit characteristics may be derived from S_n and S_c.

In the aforementioned derivation, the entire circuit has been assumed as a 2-port circuit. The characteristics of a multiport circuit may be obtained in a similar manner.

III. Optimum Design of a Ladder-Type 3-dB Hybrid— An Example of Application

To demonstrate the usefulness of the segmentation method in design problems, its application to the optimum design of a ladder-type 3-dB hybrid will be described as an example.

A. Computer Analysis

We consider a ladder-type 3-dB hybrid as shown in Fig. 3. At a frequency for which $l = \lambda_g/4$, where λ_g denotes the wave-
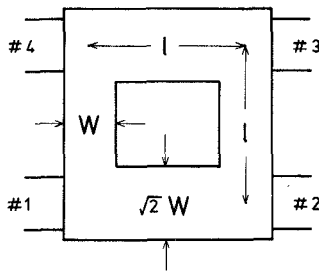
Fig. 4.   A ladder-type planar circuit which requires planar-circuit approach.
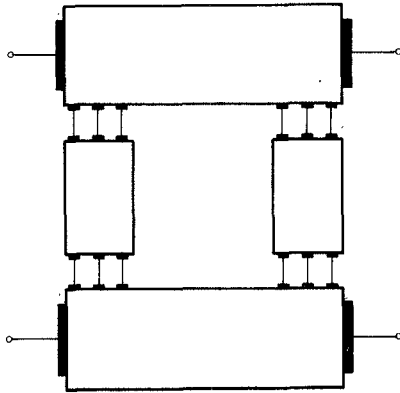

Fig. 5.   Segmentation of the ladder-type 3-dB hybrid.

length in the stripline, this circuit shows hybrid characteristics; when power is incident at port 1, it will appear at ports 2 and 3 half-and-half, and no power appears at port 4. Similar relations hold for inputs at other ports.

However, in the following two cases, the stripline width becomes comparable to the quarter wavelength as shown in Fig. 4. The first case is when the required impedance level of the hybrid is relatively low as in a mixer circuit employing Schottky-barrier diodes which have low matching impedance. The second case is when the frequency is relatively high and the length of the arms are shortened. In either case, we have to deal with the circuit as a planar circuit.

The segmentation method is most conveniently used in analyzing such a planar hybrid circuit. In the following analyses, we assume that the circuit is of triplate type, with dielectric-spacing material having ε_r (relative dielectric constant) = 2.53 and $d = 1.52$ mm, in accordance with the material used in the experiment.

We first divide the circuit into four segments as shown in Fig. 5. Next the S-matrices of each segment are computed by transforming the Z-matrices given in [1] into S-matrix form. Finally, we synthesize them by the method previously described to obtain the S-matrix of the entire 4-port.

The method of taking into account the width of external terminals (see Fig. 5) might require some comment. When the external terminals are assumed to have certain widths, components of the impedance matrix are computed by averaging the Green's function of the wave equation over the widths of the corresponding terminals [1]. When the terminal shifts, the averaging range should be moved accordingly.

B. Starting Circuit Pattern

As a starting circuit pattern, we take one as shown in Fig. 5 and assume that $l = 10.8$ mm for each arm. According to the distributed-constant model (Fig. 4), this length and $\varepsilon_r = 2.53$

lead to f_0 (center frequency) = 4.4 GHz. Further, if we assume $Z_0 = 50\ \Omega$, we obtain $W = 3.6$ mm and $\sqrt{2}\ W = 5.1$ mm. Comparison of l and W suggests that the planar-circuit model must be employed in exact analysis and design.

The result of the segmentation-method analysis of the aforementioned circuit pattern is shown in Fig. 6(b). These characteristics show increase of the center frequencies (approximately 20 percent above f_0) as well as asymmetries. Obviously, this starting circuit pattern requires improvement.

C. Figure of Merit

Starting at the aforementioned circuit pattern we look for better ones. As the figure of merit of a circuit pattern we use the "bandwidth" defined as follows: at any frequency within the "band," incident power at port 1 is divided and appears at ports 2 and 3 with percentages less than 55 percent and greater than 45 percent, and at ports 1 and 4 with percentages less than 5 percent. The circuit pattern is modified successively upon trial-and-error basis so that the "bandwidth" be maximized and the symmetry of the frequency response be optimized.

In modifying the circuit pattern, symmetries of the circuit pattern with respect to two axes remain. Hence, the circuit characteristics may be determined by four parameters: $|S_{11}|^2$, $|S_{12}|^2$, $|S_{13}|^2$, and $|S_{14}|^2$.

D. Variation of Characteristics by Modification of Circuit Pattern

To collect basic information needed in the optimization, we first investigate the variation of characteristics caused by modification of design parameters.

First, effects of the position of terminals were investigated. The computed characteristics are shown in Fig. 6(a)–(g). This figure shows that when terminals move from the ends of the $\sqrt{2}\ W$-width arms toward those of the W-width arms, the S-parameters vary as shown in Table I(a). The optimum pattern is found somewhere between Figs. 6(c) and Fig. 6(d). The obtained terminal position is shown in Fig. 7, for which the center frequencies of $|S_{11}|^2$, $|S_{12}|^2$, and $|S_{14}|^2$ show the best coincidence. Hereafter, we consider only the terminal positions shown in Fig. 7.

Next, for further improvement of the characteristics, variations caused by shortening the $\sqrt{2}\ W$-width arms were investigated. It was found that the variations as shown in Table I(b) took place. (The detailed data are omitted to save space.)

Finally, the variations caused by widening the $\sqrt{2}\ W$-width arms were investigated. It was found that the variations as shown in Table I(c) took place.

If we disregard a common shift of the center frequencies, the variations of the length and/or width of the W-width arms may be replaced by those of the $\sqrt{2}\ W$-width arms.

### E. Optimum Circuit Pattern

Based upon the aforementioned tendencies obtained by the high-speed computer analyses using the segmentation method, we performed the final optimization as follows.

1) Determine the optimum position of ports so that center frequencies of $|S_{11}|^2$, $|S_{12}|^2$, and $|S_{14}|^2$ coincide with each other (Fig. 7).
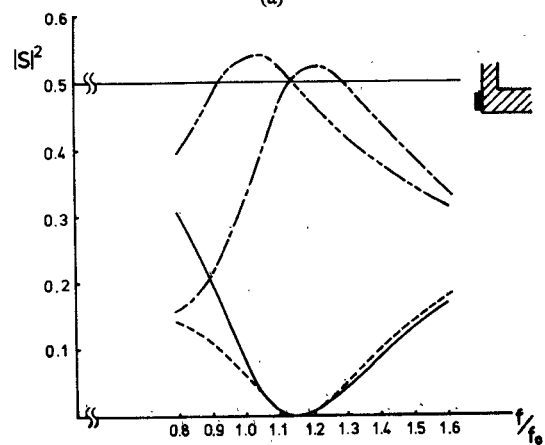
2) Determine the optimum width of the $\sqrt{2}\ W$-width arms so that the peak value of $|S_{12}|^2$ is optimized. (At this stage, the center frequency of $|S_{13}|^2$ is somewhat deviated.)
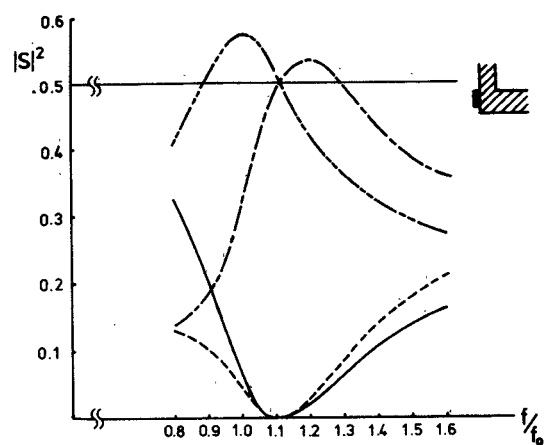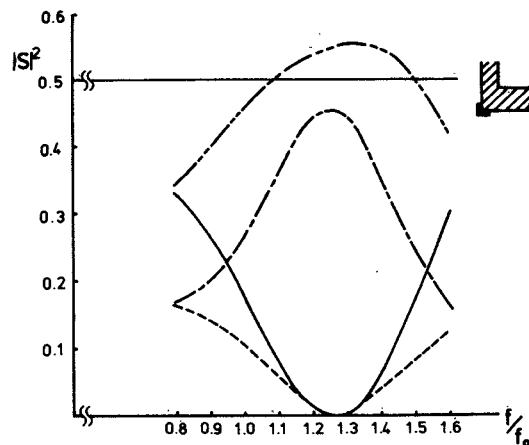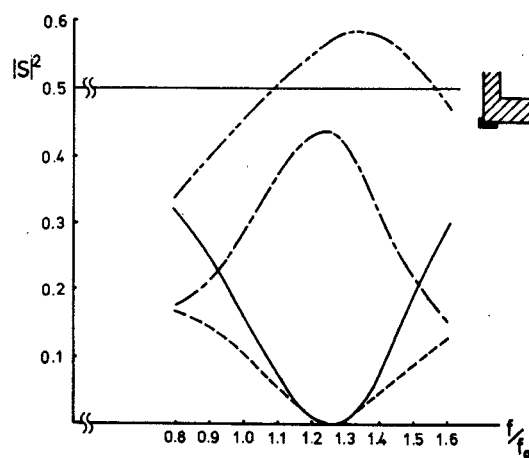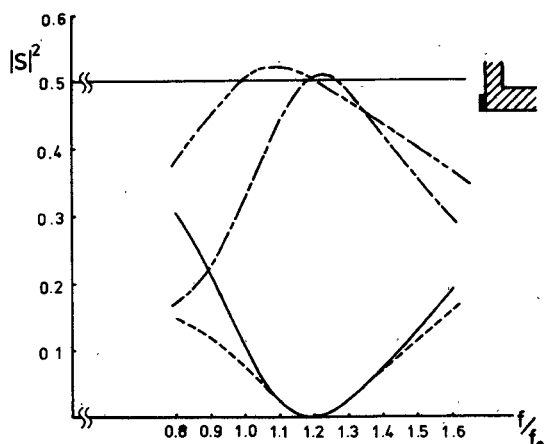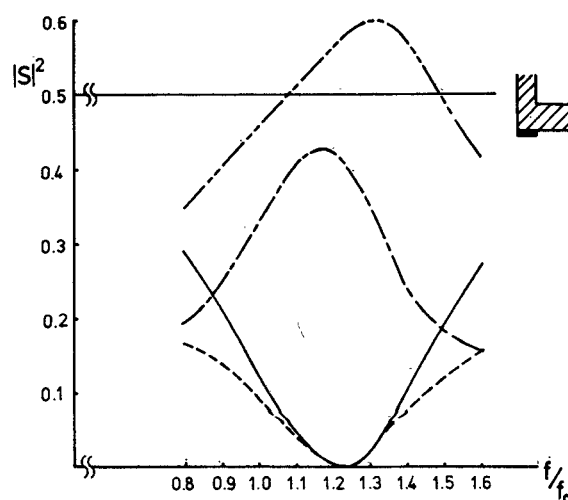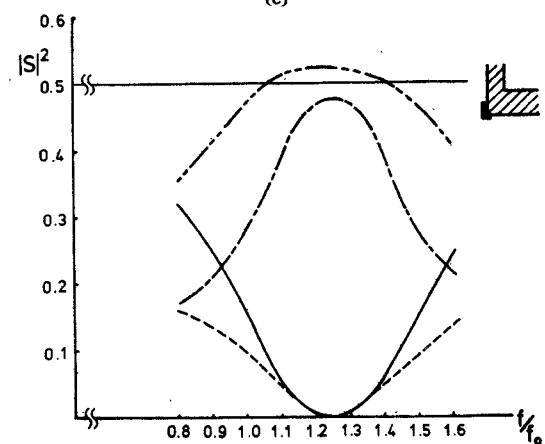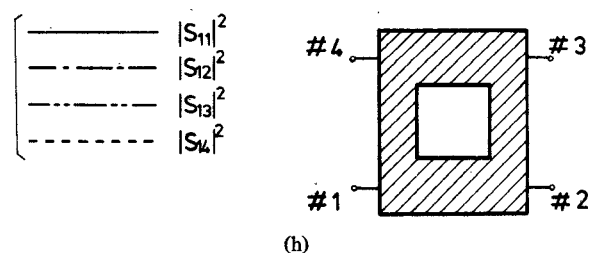
Fig. 6. Variation of the characteristics caused by the shift of terminals. (a)–(g) The corresponding terminal positions are illustrated at the right top. (h) The curve designations. Symbol f_0 denotes the center frequency based upon the distributed-constant theory.
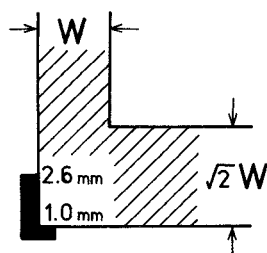
Fig. 7. The optimum terminal position.

TABLE I
VARIATIONS OF S-PARAMETERS CAUSED BY MODIFICATION OF THE CIRCUIT PATTERN

	$\lvert s_{11}\rvert^2$	$\lvert s_{12}\rvert^2$	$\lvert s_{13}\rvert^2$	$\lvert s_{14}\rvert^2$
Center frequency	↗	×	↗↗	↗
(p:peak, v:valley)	v	p	p	v
Peak or valley value	—	↘	↘↗	—

(a) Effects of the shift of terminal positions. (For their shift from ends the $\sqrt{2}$W-width arms toward those of the W-width arms.)

	$\lvert s_{11}\rvert^2$	$\lvert s_{12}\rvert^2$	$\lvert s_{13}\rvert^2$	$\lvert s_{14}\rvert^2$
Center frequency	×	×	↗↗	×
(p:peak, v:valley)	v	p	p	v
Peak or valley value	—	×	↘↗	—

(b) Effects of shortening the $\sqrt{2}$W-width arms.

	$\lvert s_{11}\rvert^2$	$\lvert s_{12}\rvert^2$	$\lvert s_{13}\rvert^2$	$\lvert s_{14}\rvert^2$
Center frequency	×	×	↗	×
(p:peak, v:valley)	v	p	p	v
Peak or valley value	—	↗↗	↘↘	—

(c) Effects of widening the $\sqrt{2}$W-width arms.

↗ : Increases gradually.
↗↗ : Increases abruptly.
↘↘ : Decreases abruptly.
↘↗ : Once decreases and then increases.
× : No remarkable variation.
— : These "valley" values are always almost zero.

3) Determine the length of the $\sqrt{2}$ W-width arms so that the center frequency of $\lvert S_{13}\rvert^2$ coincides with the others.

The optimum circuit pattern obtained finally and the corresponding circuit characteristics are shown in Fig. 8.

IV. COMPARISON WITH EXPERIMENT

Experiment was performed using the optimum circuit pattern obtained theoretically to confirm the validity of the analysis and design procedures.

A center conductor having dimensions shown in Fig. 9 was sandwiched by two ground conductors, with spacers of Rexolite 1422 ($d = 1.52$ mm, $\varepsilon_r = 2.53 \pm 0.03$). The center conductor was produced by a photoetching technique. In the analysis described in Section III, the open-circuit boundary was assumed along the edges of the circuit. Actually, however, the electromagnetic field extends outward due to the edge effect. One method to take this effect into account in the analysis is to shift all the circuit boundaries outward by $0.442d$, in this case by
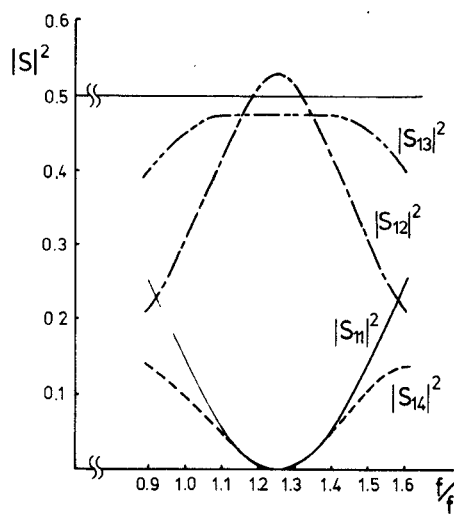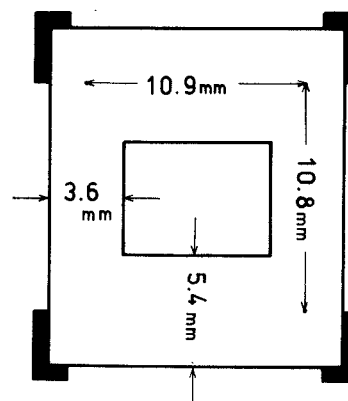

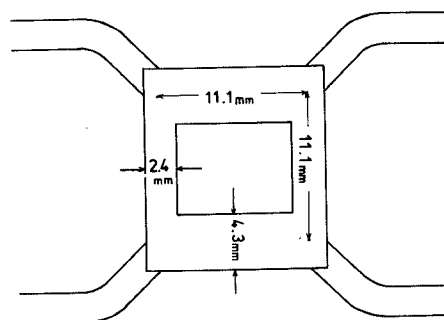Fig. 8. The optimum circuit pattern and the corresponding characteristics.

Fig. 9. The circuit pattern used in the experiment (see footnote).

0.67 mm [3]. The circuit dimensions shown in Fig. 9 were chosen so that the corrected pattern agrees with Fig. 8.[1]

The computed and measured circuit characteristics are shown in Fig. 10 by solid curves and dots, respectively. They show good agreement with each other, except for a certain loss (approximately -0.7 dB) found in the measured value of $\lvert S_{13}\rvert^2$.

V. COMPUTER TIME

A high-speed analysis technique is a premise for the trial-and-error optimum design of a microwave integrated circuit.

In the present case, the required computer time for analyzing the circuit pattern shown in Fig. 4 for a single frequency was

[1] However, due to error in the photoetching process, the measured arm lengths in the completed pattern (11.1 mm for all arms) were longer than the design value by 2 and 3 percent for the $\sqrt{2}W$-width and the W-width arms, respectively. The computed characteristics shown in Fig. 10 are based upon the actual circuit dimensions.
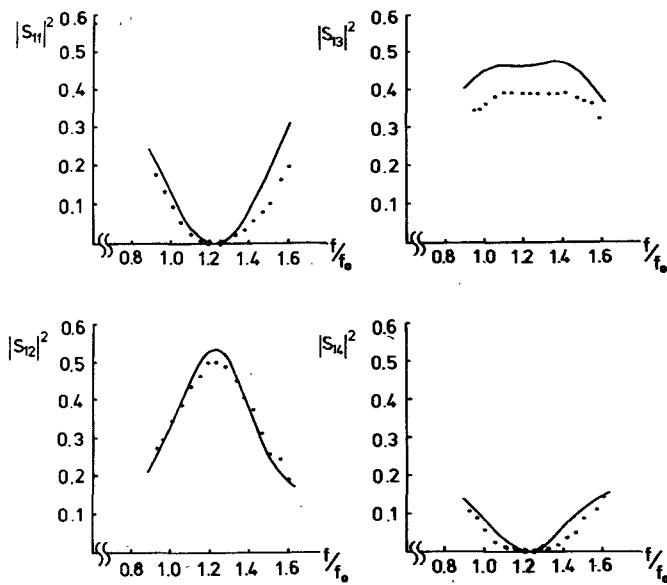
Fig. 10.   Comparison of the computed and measured circuit characteristics.
(Solid curves: computed; dots: measured.)

about 2.5 s when 10×10 modes were considered in each segment. (The computer used was a HITAC-8800.) However, by decreasing the number of considered modes to a reasonable one (for example, 8×3), the required time will easily be reduced below 0.7 s. On the other hand, when we used the contour-integral method [1], the estimated time required for the corresponding accuracy was about 5 s. ·

Generally speaking, comparison of the previous two methods is rather difficult. However, in many cases reduction of the computer time by almost an order of magnitude was possible by the segmentation method without great loss of accuracy as compared with the contour-integral method.

VI. CONCLUSION

The principle and computation procedure of an efficient method for analyzing a planar circuit, the segmentation method, was presented. To show the usefulness of the proposed method, its application to the trial-and-error optimum design of a hybrid circuit was demonstrated.

The application of the same principle to the short-boundary planar circuit, which has mainly been dealt with by contour-integral analysis [4], will be another interesting task in near future.

ACKNOWLEDGMENT

The authors wish to thank Prof. Y. Okabe of University of Tokyo for his helpful advice, and Prof. J. P. Hsu of Kanagawa University and his colleagues for their assistance in preparing the circuit used in the experiment.

REFERENCES

[1] T. Okoshi and T. Miyoshi, "The planar circuit—An approach to microwave integrated circuitry," *IEEE Trans. Microwave Theory Tech.*, vol. MTT-20, pp. 245–252, Apr. 1972.
[2] P. Silvester, "Finite element analysis of planar microwave networks," *IEEE Trans. Microwave Theory Tech.*, vol. MTT-21, pp. 104–108, Feb. 1973.
[3] N. Marcuvitz, *Waveguide Handbook*. New York: McGraw-Hill, 1951, p. 160.
[4] T. Okoshi and S. Kitazawa, "Computer analysis of short-boundary planar circuits," *IEEE Trans. Microwave Theory Tech.*, vol. MTT-23, pp. 299–306, Mar. 1975.

Temperature Compensation of TE011-Mode Circular Cavities

ALI E. ATIA, MEMBER, IEEE, AND
ALBERT E. WILLIAMS, MEMBER, IEEE

Abstract—This short paper describes a novel method for temperature compensation of TE011-mode circular-waveguide cavities. Implementation and experimental results on a single cavity are presented.

INTRODUCTION

Temperature compensation of TE011-mode circular cavities has been attempted previously for applications related to wavemeter construction (see [1, secs. 6.22 and 6.25]). The basic idea of temperature compensation is to provide opposite changes in cavity length and diameter with temperature changes so that the resonant frequency remains constant. For cavities intended for operation at a fixed center frequency, it is easily shown that compensation is feasible. The resonant frequency of a cylindrical cavity excited in the TE$_{lmn}$ mode is given by

$$f = \sqrt{\left(\frac{cx_{lmn}}{\pi D}\right)^2 + \left(\frac{cn}{2L}\right)^2} \tag{1}$$

where c is the speed of light, x_{lmn} is the proper root of the Bessel function corresponding to the mode under consideration, and L and D are the length and diameter of the cavity at temperature T_0, respectively. The incremental change Δf in the resonant frequency f due to changes ΔL and ΔD in the cavity dimensions is obtained from (1) by taking its total differential

$$\Delta f = -\frac{(xc_{lmn}/\pi D)^2(\Delta D/D) + (cn/2L)^2(\Delta L/L)}{f}. \tag{2}$$

This change will be zero if

$$\frac{(\Delta L/L)}{(\Delta D/D)} = -\left(\frac{2x_{lmn}L}{n\pi D}\right)^2. \tag{3}$$

Fig. 1 shows a possible implementation of the temperature compensation scheme. The noncontacting tuning plunger is constructed from two disks of the same cavity metal (having linear temperature-expansion coefficient α_c) sandwiching a material with a higher thermal coefficient of expansion (α_p) and a thickness t at the ambient temperature. It can easily be seen that, for the TE011 mode, (3) is satisfied if the linear temperature coefficients of expansions α_p and α_c are related by

$$\frac{\alpha_p}{\alpha_c} = 1 + \left(\frac{L}{t}\right)\left\{1 + \left(\frac{2x_{011}L}{n\pi D}\right)^2\right\}. \tag{4}$$

EXPERIMENTAL RESULTS

An experimental TE011-mode circular cavity has been constructed with the tuning plunger designed as in Fig. 1. The cavity material is aluminum and the high-expansion material is a commercially available silicone resin ($\alpha_p \approx 30\alpha_c$). The experimentally measured resonant-frequency shifts of the uncompensated and compensated cavities with temperature are shown in Fig. 2. It can be seen that the 12-GHz compensated cavity has a maximum shift of about 1.5 MHz in a temperature excursion of 100°C. This shift is less than that which would be obtained from a corresponding uncompensated Invar cavity.